RSC Advances

PAPER

View Article Online
View Journal | View Issue

Cite this: *RSC Adv.*, 2020, **10**, 10118

Preparation and biological properties of silk fibroin/nano-hydroxyapatite/graphene oxide scaffolds with an oriented channel-like structure

Lu Wang,† Min Fang,† Yijing Xia, Jiaxin Hou, Xiaoru Nan, Bin Zhao* and Xiangyu Wang*

Constructing an ideal bone tissue engineering scaffold has been one of the research hotspots in the biomedical field. Silk fibroin (SF), nano-hydroxyapatite (nHAp) and graphene oxide (GO) are excellent biomaterials, and have been studied and explored extensively. To better mimic natural bone, we fabricated a SF/nHAp/GO hybrid scaffold with an oriented channel-like structure by using directional temperature field freezing technology. A comparative analysis was carried out for the SF, SF/nHAp, unoriented SF/nHAp/GO and oriented SF/nHAp/GO scaffolds. The physical and chemical properties were studied by scanning electron microscopy, X-ray diffraction, Fourier transform infrared spectroscopy and universal mechanical testing. The data showed that the oriented channel-like SF/nHAp/GO porous scaffold expressed high interconnectivity, suitable pore diameter and porosity and anisotropic mechanical properties. Cytocompatibility tests indicated that the oriented channel-like SF/nHAp/GO porous scaffold was more favorable for stimulating bone marrow mesenchymal stem cells (BMSCs) adhesion and proliferation. Additionally, human umbilical vein endothelial cells (HUVECs) grew unimpeded along the channel, indicating it had advantages for vascularization. For further testing *in vitro*, osteogenic induction was carried out on BMSCs inoculated on the above scaffolds, and then alkaline phosphatase (ALP) activity was tested and cell mineralization was observed. The results indicated that the oriented channel-like SF/nHAp/GO porous scaffold was more conducive to osteogenic differentiation of BMSCs. Hence, the material may prove to be a promising scaffold for bone tissue engineering.

Received 20th November 2019
Accepted 24th February 2020

DOI: 10.1039/c9ra09710d

rsc.li/rsc-advances

1. Introduction

Biomedical scientists have been devoted to investigating new biomaterials for bone tissue engineering with innovative properties for many years. An ideal scaffold can provide an appropriate microenvironment for cell adhesion, proliferation and differentiation and ultimately induce normal gene expression as well as guiding tissue regeneration. Consequently, it is still urgent to construct a new type of bone repair scaffold with excellent biocompatibility, stable physics and chemical properties and osteoinduction activity.

The composition and pore structure have always been the focus during the scaffold designing and preparation process, because they really play a crucial role in the effect of tissue repair and regeneration. Accordingly, we emphasize the composition in the first step to construct the scaffold. Silk fibroin (SF), derived from *Bombyx mori* cocoons, is a commonly available natural biopolymer with a long history of applications in the human body as sutures. With the deep understanding of its intrinsic properties such as mechanical strength, elasticity, biocompatibility and controllable biodegradability, SF has been fabricated into films,[1] scaffolds,[2] hydrogels[3] or non-woven mats,[4] and these SF-based materials have been widely used for tissue engineering scaffold.[5–8] Unfortunately, SF materials with single component are lacking osteoinductive activity and this defect greatly hinders the application of SF in bone repair field. Hydroxyapatite (HAp) is a representative bioactive ceramic material with good biocompatibility and osteo-induction capacity. Its chemical composition and crystal structure are similar to those of natural bone. Nano-hydroxyapatite (nHAp) has higher biological activity,[9,10] which can provide necessary conditions for bone conduction, protein adhesion and bone regeneration. Although hydroxyapatite is the most common alternative material in bone defect repair, its application is greatly restricted by the difficulty of shaping and brittleness. Therefore, plenty of composite scaffolds including HAp/collagen,[11] HA/poly-lactic acid (PLA),[12] HA/poly-caprolactone (PCL),[13] HA/poly(lactic-*co*-glycolic) acid (PLGA),[14] have been developed for bone repair and regeneration. Undoubtably, HAp/SF composite is no exception. The relationship between SF and HAp is very interesting. On the one hand, the SF molecular

School and Hospital of Stomatology, Shanxi Medical University, Taiyuan 030001, China. E-mail: sxmu0688@126.com; wangxiangyu76@163.com; Tel: +86-351-4690868

† These authors contributed equally to this paper.

chains can provide nucleation sites for HAp, on the other hand, the nucleation of HAp can promote the ordered arrangement of SF molecular chains, which can enhance the osteogenic activity of the composite scaffold, and also make up for the defects of HAp effectively.[15] Graphene oxide (GO), a single layer of sp^2-bonded carbon atoms, has demonstrated great application prospects in tissue engineering. It has unique structure, outstanding mechanical property and high thermal and electrical conductivity. Recently, GO has been confirmed to be effective in bone regeneration, because it has the ability to induce osteogenic differentiation of stem cells and greatly enhance the nucleation and crystallization of HAp.[16,17] Furthermore, many studies have shown that GO always serve as an excellent reinforcement nanofiller and increase the mechanical properties of the composite material significantly, which could result in a stiff surface that is beneficial to the growth and proliferation of osteoblasts.[18,19]

The pore structure of the scaffold is another key factor concerned in this study. A large number of studies have shown that pore size, porosity and pore connectivity are important structural parameters affecting the biological properties including cell migration and bone inward growth.[20,21] Although traditional sponge-like scaffolds have been widely studied and used, the smaller diameter of the channel pore between adjacent macropores, usually leads to lower pore connectivity and peripheric new bone formation instead of growth into the inner porous structure, mainly produce irregular woven bone.[22] Additionally, unlike the anisotropy of natural bone, the spongy scaffolds exhibit isotropic stress transmission, which may impede their integration with the host bone.[23] In recent years, researchers have been inspired by the unique parallel channel structure in lotus root, and a new type of scaffold with oriented channel-like structure has been prepared. The studies[24–26] show that the oriented channel-like scaffold is more beneficial to the release of oxygen and nutrients due to its higher pore connectivity and lower flow resistance. Moreover, oriented channel-like scaffold has anisotropy stress, which is closer to the characteristics of natural bone, can promote cell migration and facilitate the formation and functionalization of normal tissue on its morphology and structure. Besides, such oriented channel-like structure can induce endothelial cells to form basic vascular structure, and as is known to all, vascularization plays a really important role in the process of new bone formation.

The past several years have witnessed the explosion of SF, HAp and GO research in a variety of different field. With the development of more advanced scaffold fabrication techniques, such as solvent-casting, gas-foaming, emulsion freeze-drying, electrospinning and 3D printing, a few scaffolds compounded by any two of SF, HAp and GO or all of the three have emerged. Studies have shown the composite utilization of the SF, HAp and GO materials can usually enables them to play a synergistic role in promoting cell proliferation or tissue regeneration. Li *et al.* successfully deposited ternary SF/GO/HAp nanocomposite coatings on Ti substrate by exploiting electrophoretic nanotechnology. The study suggested that SF/GO/HAp nanocomposite coatings could be a promising candidate for the surface functionalization of biomaterials, especially as orthopedic implant coating.[27] In another study, to better mimic natural bone, a cGO-HAp/SF scaffold was fabricated by biomineralizing carboxylated GO sheets, blending with SF, and freeze-drying. The cGO-HAp/SF composite exhibited more superior mechanical properties and biocompatibility than HAp/SF and pure HAp scaffolds, which may proved to be an excellent and versatile scaffold for bone tissue engineering.[28] But these studies ignored the synergistic effect of composition and structure on the properties of the composites.

Based on the above theory and previous studies, we plan to make a further study on the joint application of the SF, HAp and GO, here we study the potential use of SF/nHAp/GO composites with different pore structure as scaffolds in bone tissue engineering. The morphology, condensed structure and mechanical properties were characterized, which could provide some useful evidence for the synergistic effect of three components in the scaffold. Furthermore, the biological performance after seeding them with bone marrow mesenchymal stem cells (BMSCs) and human umbilical vein endothelial cells (HUVECs) was also described. We hope the SF/nHAp/GO hybrid scaffold can be employed as a competitive scaffolding option for bone tissue regeneration.

2. Experimental section

2.1 Materials

Bombyx mori raw silk fibers were purchased from Dingsheng Silk Co. Ltd (Wujiang, China). Graphene oxide was purchased from XFNANO Materials Tech Co. Ltd (Nanjing, China). Bone marrow mesenchymal stem cells were extracted from the leg bone marrow of experimental rats. Human umbilical vein endothelial cells were purchased from TongPai Biological Tech Co. Ltd (Shanghai, China). Dulbecco's Modified Eagle's Medium (DMEM), RPMI-1640 medium and fetal bovine serum (FBS) were purchased from Gibco Invitrogen. Dexamethasone, L-ascorbic acid and β-glycerophosphate were purchased from Cyagen Biological Tech Co. Ltd (Guangzhou, China). Cell Tracker CM-DiI (Molecular Probes, Invitrogen) was purchased from Wegene Biological Tech Co. Ltd (Shanghai, China). Cell Counting Kit-8 was purchased from Boster Biological Tech Co. Ltd (Wuhan, China). Calcium Detection Assay kit (colorimetric) and Glycerol (G-2025) were purchased from Sigma-Aldrich Trading Co. Ltd (Shanghai, China). All materials and reagents were used as received with no further purification.

This study was performed in strict accordance with the NIH guidelines for the care and use of laboratory animals (NIH publication no. 85-23 rev. 1985) and was approved by the Institutional Animal Care and Use Committee of National Tissue Engineering Center (Shanghai, China). Furthermore, it was performed by complying with the institutional regulations established and approved by the Medical Ethics Committee at Stomatological Hospital of Shanxi Medical University. All the rats were purchased from the laboratory animal center of Shanxi Medical University.

2.2 Fabrication of scaffolds

2.2.1 Preparation of the SF, GO solution. According to published methods, cocoons were degummed three times in

0.5 wt% Na_2CO_3, dissolved in $CaCl_2$, ethanol, and distilled water at molar ratio 1 : 2 : 8, and stirred at 72 °C for 1 h. The solution was dialyzed for 4 days in deionized water and filtered to remove undissolved parts to obtain regenerated SF (2 wt%). The solution was concentrated to 5 wt% in oven at 60 °C. GO powder was dispersed in distilled water by ultrasonication for 30 minutes, adjusting the GO concentration for 2 mg ml^{-1}. The pH value of the GO suspension was modulated to 10 by sodium hydroxide solution (1 mol l^{-1}).

2.2.2 Fabrication of SF, SF/nHAp and SF/nHAp/GO scaffolds. Firstly, SF solution (5 wt%) were poured into three beakers, then nHAP powder and GO suspension were added into SF solution at a ratio of 10 wt% and 0.5 wt% against to the weight of SF, respectively. After 5 minutes of ultrasonic oscillation, three groups of homogeneous solution were obtained. Glycerol was used as the cross-linking agent to obtain the insoluble scaffolds. The three groups of mixed solution were injected into several glass dishes, frozen at −20 °C for 24 h, followed by lyophilization for 48 h to form the SF, SF/nHAp and SF/nHAp/GO porous scaffolds.

2.2.3 Fabrication of SF/nHAp/GO hybrid scaffold with oriented channel-like structure. Based on the principle of the directional temperature field freezing technology, the SF/nHAp/GO solution prepared by the above method was injected into some silicone tubes at a diameter of 8 mm and a height of 1 cm. The bottoms of silicone tubes contacted closely to a extreme cold surface, and the tops were exposed. These solution were frozen at −80 °C for 24 h and lyophilized for 48 h. Finally, SF/nHAp/GO hybrid scaffolds with oriented (from bottom to top) channel-like structure were obtained.

2.3 Characterizations

2.3.1 Scanning electron microscopy (SEM). SEM was used to examine the surface/cross-sectional pore morphology of composite scaffolds. All the porous scaffolds were repeatedly soaked with deionized water to remove glycerin, and then subjected to secondary freeze drying. The samples were coated with gold with sputter coating in vacuum before analysis and observed using a field-emission scanning electron microscope (SEM, JEOL, Japan). The pore sizes were determined by averaging random 50 pores from the SEM images.

2.3.2 Structure analysis by XRD and FT-IR. The crystalline structures and presence of phases of the various scaffolds were analyzed by X-ray diffraction (XRD) on Miniflex II (Rigaku, Japan) diffractometer with Cu Kα radiation (λ = 1.54178 Å), measured with 2θ ranging from 5°to 45°and the Fourier transform infrared (FT-IR) spectroscopy which was preformed *via* a spectrometer of TENSOR II (Bruker, Germany) in the range of 4000–400 cm^{-1}. Prior to analysis, all samples were cut into micro-particles.

2.3.3 Porosity measurement. The porosity of the scaffolds was measured by liquid displacement, using ethyl alcohol as the displacement liquid. A pre-weighted dry sample was immersed in a defined volume (V_1) of ethyl alcohol in a graduated cylinder for 10 min. The total volume of the ethyl alcohol and the ethyl alcohol impregnated scaffold was recorded as V_2. Then the ethyl alcohol impregnated scaffold was removed from the graduated cylinder and the residual ethyl alcohol volume was recorded as V_3. The porosity of the scaffold was expressed as: porosity (%) = $(V_1-V_3)/(V_2-V_3)$.

2.3.4 Mechanical properties. SF, SF/nHAp, SF/nHAp/GO porous scaffolds were fabricated into inerratic samples in size of 10 mm × 10 mm × 10 mm, and indentation tests were carried out by using a computer controlled universal testing machine (Instron5544, America). Took the head with a diameter of 1 mm and pressed the samples to 1/10 of the initial thickness at a speed of 0.2 mm min^{-1}, then stopped. Five samples were tested in each of the three groups, and the compressive strength and elastic modulus of the scaffolds were finally calculated by the following formula.

$$E = \frac{F(1-\nu^2)}{2R\delta} \quad (F: \text{pressure}, \nu: \text{Poisson ratio}, R: \text{head radius}, \delta: \text{displacement})$$

$$P = \frac{E\delta}{\pi R^2(1-\nu^2)} \quad (E: \text{elastic modulus}, \delta: \text{displacement}, R: \text{head radius}, \nu: \text{Poisson ratio})$$

The compressive strength of the oriented SF/nHAp/GO porous scaffold (10 × 10 × 10 mm^3) with different directions were tested at a cross-head speed of 0.5 mm min^{-1}, and the load was applied until the specimen was compressed to approximately 40% of its original length.

2.3.5 Cell compatibility *in vitro*. The various scaffolds with a diameter of 8 mm were placed in the 48-well tissue culture plates (Corning Inc., USA), sterilized by γ-ray irradiation and rinsed with sterilized PBS prior to cell seeding.

At the first stage, BMSCs were used to evaluate the cell compatibility of the several scaffolds served as options for bone tissue engineering. After ∼80% confluence, the BMSCs suspension (a density of 2 × 10^4 cells per ml) was loaded onto the scaffolds in the 48-well plates and incubated at 37 °C in a humidified atmosphere of 95% air and 5% CO_2. To investigate the distribution of BMSCs in the scaffolds, the cells were labeled by CM-DiI dye (2 mg ml^{-1}). The medium in each well was refreshed every 2 days. The viability and morphology of the BMSCs seeded on the scaffolds were assessed by CCK-8 assays, and laser scanning confocal microscopy (LSCM, Olympus, FV1000, Japan) on day 2, 5 and 10.

Then at the second stage, HUVECs were used to evaluate the effect of oriented channel-like structure on vascularization. In this stage, the HUVECs suspension (a density of 2 × 10^4 cells per ml) was loaded onto the traditional SF/nHAp/GO porous scaffolds and the novel oriented channel-like ones in the 48-well plates and incubated at 37 °C in a humidified atmosphere of 95% air and 5% CO_2. The medium in each well was still replaced every 2 days. After incubation for 3 and 7 days, we observed the viability and morphology the same as above.

2.3.6 Osteogenic differentiation of BMSCs. For osteogenic differentiation, the 3rd generation BMSCs suspension (a density of 2×10^4 cells per ml) was loaded onto the scaffolds in the 48-well plates. After one day's culture in DMEM basic medium, the DMEM osteogenic differentiation medium supplemented with 10% FBS, 10 nM dexamethasone, 100 mM L-ascorbic acid, and 10 mM β-glycerophosphate were added. The medium in each well was refreshed every 2 days. In order to detect the osteogenic activity of BMSCs induced on the scaffolds, a quantitative detection of ALP activity was tested on day 7, 10 and 14 and calcium deposited in the ECM was measured by Calcium Detection Assay kit (colorimetric) on day 10, 14 and 21.

2.4 Statistical analysis

Statistical comparisons were performed using SPSS 20.0 statistical software. Data were reported as mean ± standard deviation where indicated, and were analyzed by *t*-test and one-way classification ANOVA. The differences at $P < 0.05$ were considered statistically significant.

3. Results and discussion

3.1 Morphology and pore structure

Over the years, there have been several theories about the effects of porous scaffolds on cell growth. It was reported that scaffolds with pore diameter of 100–300 μm were beneficial to the proliferation and osteogenic differentiation of BMSCs.[26,29] Some scholars pointed out that the "bottleneck" restricting the growth of bone tissue into the pores is not the diameter of the pores, but the degree of interconnection between the pores and the size of the channel between the pores.[30]

The morphology of the composite scaffolds were observed by SEM. Fig. 1a–c showed the microstructure of the unoriented porous scaffolds with different compositions. All scaffolds exhibited good homogeneity with continuous and interconnected pore structure and there was no visible phase separation, indicating good compatibility among SF, nHAp and GO. However, there still had some obvious differences between each scaffold. Firstly, compared with the smooth pore surface of the single component SF scaffold, the pore surface became rough after nHAp was added. These tiny particles dispersed uniformly and adhered closely to the pore walls of SF scaffolds, which increased the roughness of pore surface. Secondly, the pore structure changed more elliptical and the scaffolds exhibited an improved porous structure when GO was added. Furthermore, by calculation and comparison, we found the average pore diameter decreased from 137.2 ± 1.2 μm to 91.5 ± 1.8 μm (Table 1) and the uniformity of the pore size was enhanced with the addition of GO. Freeze-drying is a commonly-used dehydration method to dry porous scaffolds by sublimating the ice particles formed during the freezing process. The size of ice particles is affected by a few factors such as the growing of ice crystals, growing time and growing history, *etc.*[31] We found that when GO was incorporated into the SF solution, the viscosity of the blend solution was increased. This may be the consequence of active groups such as hydroxyl (═OH), carboxyl (═COOH) and epoxy (═O═) in GO and nano-size effect of GO. The large surface area, nano-sheets structure and active groups of GO can increase the interaction between components of the solution system, which is favor to increase the viscosity of the solution. Because of this, the free movement of water molecule become difficult and slow, increasing the resistance of forming larger ice particles. As a result, the pore diameter decreased with the addition of GO.

The porosity of the three unoriented scaffolds was measured as 80–83% around, regardless of the variables studied (Table 1). Such pore structure was adequate for the migration and proliferation of cells, as well as vascularization. The oriented channel-like SF/nHAp/GO hybrid scaffold were qualified with structural characteristics as above. Its pore diameter was 125.3 ± 2.1 μm, and unlike the unoriented scaffolds, their inner vertical channels (Fig. 1e) endowed the scaffold with higher interconnection, promoting the porosity dramatically (up to 90.5%) (Table 1).

3.2 Structure analysis

The crystalline structure and molecular conformation of the scaffolds were determined by XRD and FT-IR. The principal diffraction peaks of the silk I structure are at 12.2°, 19.7°, 24.7° and 28.2°, while silk II structure at 9.1°, 18.9°, 20.7° and 24.3°.[32] Both the SF sample and the hybrid samples showed an obvious peak at 20.7° (Fig. 2A(a–d)), indicating a typical silk II structure. Besides, there also appeared a principal diffraction peak at 32°, which belongs to nHAp (Fig. 2A(b–d)). Moreover, no obvious diffraction peak of GO was found in the SF/nHAp/GO scaffolds' XRD patterns (Fig. 2A(c and d)), presumely due to GO's content was low and its uniform dispersion.

Fig. 2B illustrated the FT-IR spectrum of the scaffolds. According to previous studies, for SF, the absorption bands of FT-IR spectrum were at 1650–1655 cm^{-1} (amide I), 1525–1540 cm^{-1} (amide II), 1266 cm^{-1} (amide III), and 669 cm^{-1} (amide V) are characteristics of the silk I secondary structure, the bands at 1620–1635 cm^{-1} (amide I), 1530 cm^{-1} (amide II), 1230–1235 cm^{-1} (amide III), and 700 cm^{-1} (amide V) are from the silk II structure, and those at 1655–1660 cm^{-1} (amide I), 1535–1545 cm^{-1} (amide II), 1235 cm^{-1} (amide III), and 650 cm^{-1} (amide V) are indicative of the random coil conformation.[32] In the above FT-IR spectrum, strong bands at 1233 cm^{-1}, 1530 cm^{-1} and 1647 cm^{-1} were observed, indicating a predominant silk II conformation and a few silk I secondary structure. Neither special diffraction peaks nor abnormal absorption bands existed, that showed the SF, nHAp and GO had achieved a good combination and nHAp, GO both dispersed uniformly in the SF matrix without aggregation.

3.3 Mechanical properties

The mechanical properties of the scaffolds were evaluated using indentation test and the results were shown in Fig. 3. When nHAp was added alone, the maximum compressive stress and mean elastic modulus of the SF/nHAp scaffold were up to 40.2 kPa, 123.5 kPa, higher than those of the pure SF scaffold (20.1 kPa, 70.3 kPa) (Fig. 3(A) and (B)). As is known HAp is brittle

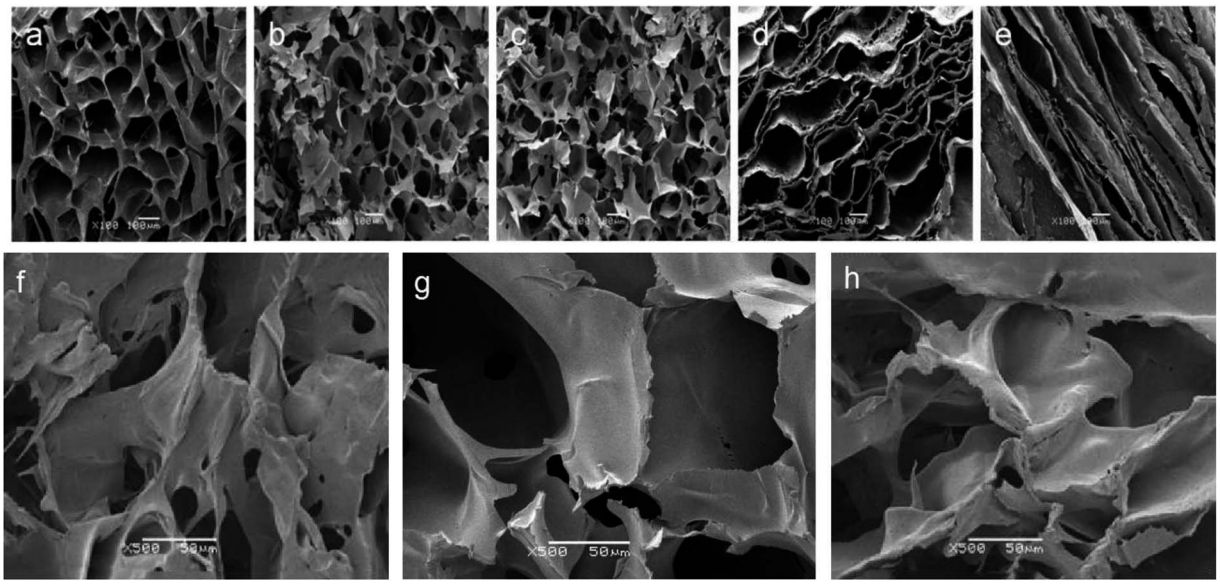

Fig. 1 SEM images of unoriented and oriented porous scaffolds. (a) SF (b) SF/nHAp (c) unoriented SF/nHAp/GO (d) cross-section of oriented SF/nHAp/GO. (e) Longitudinal-section of oriented SF/nHAp/GO (×100) (f) SF (g) SF/nHAp (h) unoriented SF/nHAp/GO (×500).

Table 1 Pore diameter and porosity of the scaffolds

Group	Pore diameter (μm)	Porosity (%)
SF	137.2 ± 1.2	83.4 ± 0.5
SF/nHAp	108.3 ± 2.3	82.3 ± 0.8
Unoriented SF/nHAp/GO	91.5 ± 1.8	80.7 ± 0.3
Oriented SF/nHAp/GO	125.3 ± 2.1	90.5 ± 1.1

and difficult to be shaped. However, when it is compounded with polymer, it will not only overcome the shortcomings above, but also improve the biocompatibility and biological activity of polymer materials. Especially when the particle size reaches nano-level, the composites can transfer the external stress better, thus improving their mechanical strength. Furthermore, with the large specific surface area, nanospherical particles form extensive contact with polymers, thus making them easier to bond firmly. Moreover, nanospherical particles can disperse stress well due to larger curvature, which can effectively prevent the dislocation movement of the matrix.[33] Therefore a property-improved SF/nHAp scaffold was acquired. GO shows high mechanical properties in recent researches, which allow it to be potential reinforcing materials for polymers. It also contains a wide range of hydrophilic groups. These functional groups allow good dispersion of GO in water, and expand the applying area. Herein, GO and nHAp were added in SF-based scaffold simultaneously, and results showed they significantly increased the compressive stress and elastic modulus of the composite scaffold. The values reached to 70.2 kPa, 212.5 kPa respectively

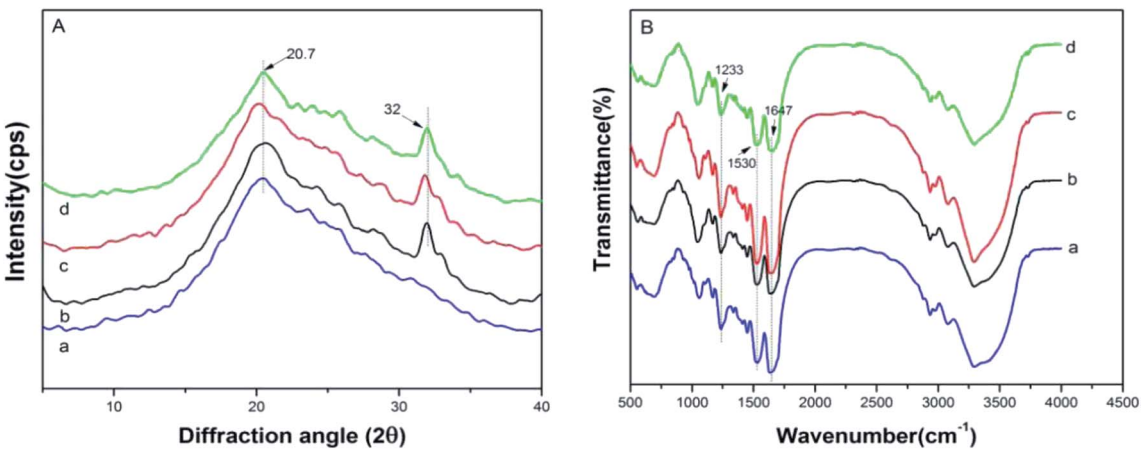

Fig. 2 XRD (A) and FT-IR (B) of SF, SF/nHAp, unoriented SF/nHAp/GO and oriented SF/nHAp/GO scaffolds. (a) SF (b) SF/nHAp (c) unoriented SF/nHAp/GO (d) oriented SF/nHAp/GO.

at 0.5 wt% GO concentration. Clearly, the addition of GO and nHAp played the role on improving the mechanical strength of the scaffold synergistically. The enhancement of the mechanical properties was related to the uniform dispersion of GO with high elastic modulus in the SF matrix and the intermolecular forces formed between the SF, nHAp and GO nanosheets. The mechanical properties of oriented SF/nHAp/GO scaffold were shown in Fig. 3(C). The compressive strength and elastic modulus are 26.37 kPa and 83.86 kPa respectively when stress applied perpendicular to pore orientation. However, the vertical data increased to 75.71 kPa and 279.73 kPa, respectively, when stress applied parallel to the pore orientation. The mechanical properties of the oriented SF/nHAp/GO scaffold exhibit anisotropic due to the pore orientation.

Generally speaking, in bone tissue engineering, the scaffold mainly undertake providing an appropriate micro-environment for the cells growth and proliferation and finally obtaining regenerated tissues, such mechanical strength of the above scaffolds can meet the needs of bone tissue scaffold in bone repair. It is worthy noting that the anisotropic of the oriented SF/nHAp/GO scaffold was another critically important factor in bone regeneration process. Wolff's law states that bone can respond to mechanical stimulation to change its apparent density and the direction of trabecular bone distribution, indicating that bone remodeling is an anisotropic behavior. The oriented SF/nHAp/GO scaffold just mimiced this characteristic of bone, giving it an advantage in bone regeneration over traditional spongy scaffolds.

3.4 *In vitro* studies

Bone scaffolds for implantation should be biocompatible and should promote cell proliferation without provoking an immune response. In current study, to evaluate cytocompatibility, BMSCs were seeded on unoriented SF, SF/nHAp, SF/nHAp/GO and oriented SF/nHAp/GO porous scaffolds. LSCM was performed to observe the distribution and attachment within the scaffolds as opposed to the surface. CCK8 assays were used to reflect cell viability and proliferation on different scaffolds.

Fig. 4 LSCM images showed the morphology of BMSCs seeded on different scaffolds. The red fluorescent highlights indicated labeled living cells. It could be seen that the cells dispersed uniformly and intimately adhere to the wall of the porous scaffolds, performing an obvious proliferation trend as the culture time prolonged. However, as far as the three unoriented porous scaffolds were concerned, the cell proliferation in

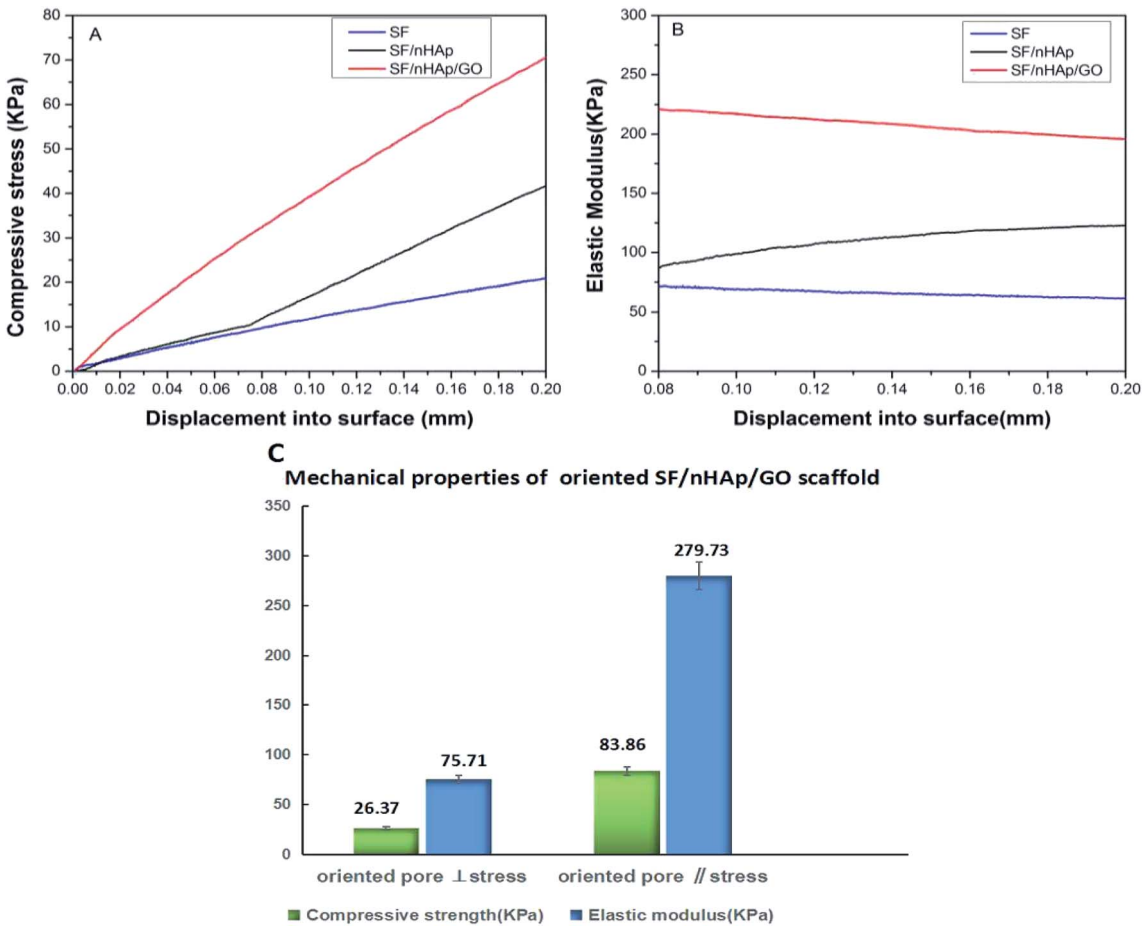

Fig. 3 Compressive stress (A) and elastic modulus (B) of SF, SF/nHAp, unoriented. SF/nHAp/GO scaffolds. Mechanical properties (C) of oriented SF/nHAp/GO scaffold.

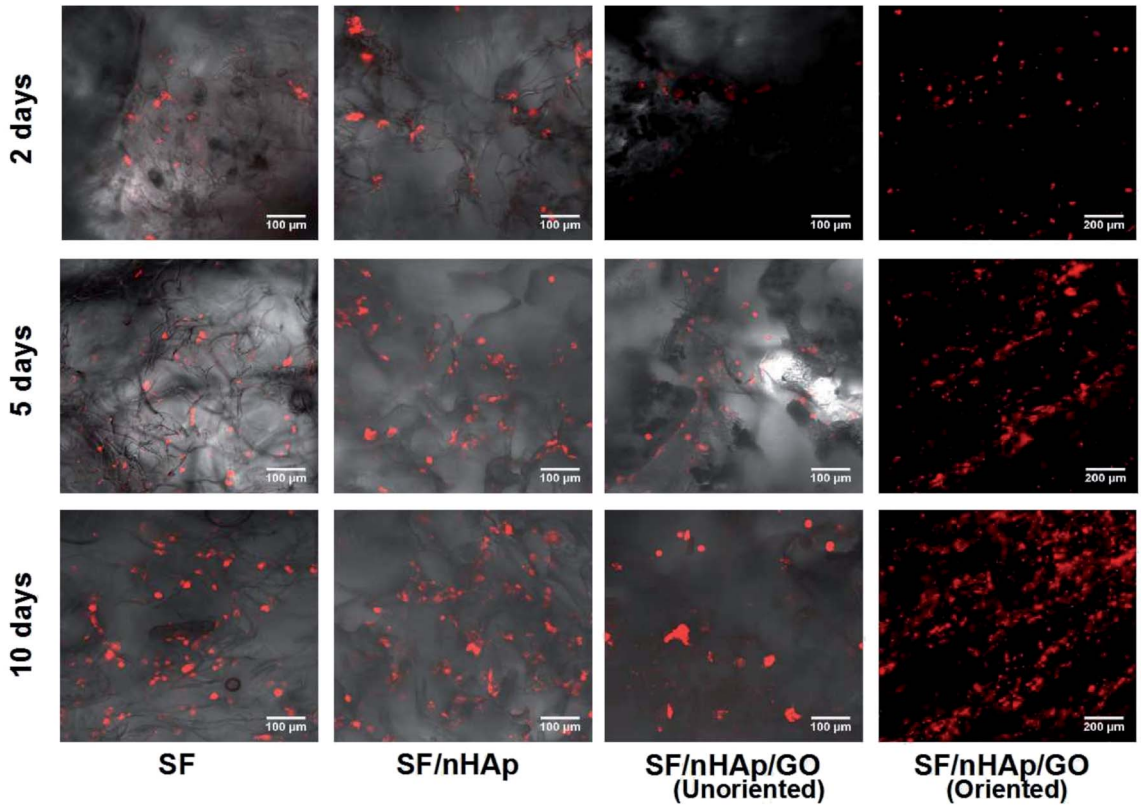

Fig. 4 LSCM images to show BMSCs cultured on different scaffolds for 2, 5 and 10 days.

SF/nHAp scaffolds was higher compared with in SF and SF/nHAp/GO porous scaffolds. Cells cultured on the oriented SF/nHAp/GO porous scaffolds distributed along vertical channels, and the proliferation rate was significantly higher than that of the unoriented ones. SEM images (Fig. 5) showed that after 10 days' cultivation on these scaffolds, BMSCs attached to the walls of pores tightly and were surrounded by extracellular matrix.

CCK8 assay (Fig. 6) indicated that there are no significant differences in cell proliferation among scaffolds on day 2. However, the number of cells cultured on unoriented SF/nHAp and oriented SF/nHAp/GO scaffolds were higher than on the SF and SF/nHAp scaffolds after 5 d. Although proliferation was comparable, the number on oriented SF/nHAp/GO scaffold was the highest ($P < 0.05$).

In brief, LSCM images and CCK8 results showed that the cell viability in the scaffolds with moderate amount of nHAp

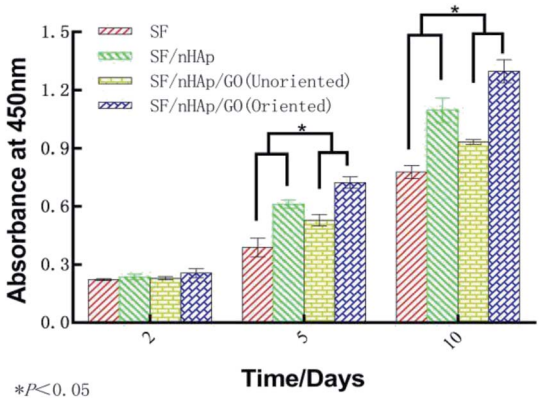

Fig. 6 OD Values of BMSCs cultured on the different scaffolds for 2, 5 and 10 days.

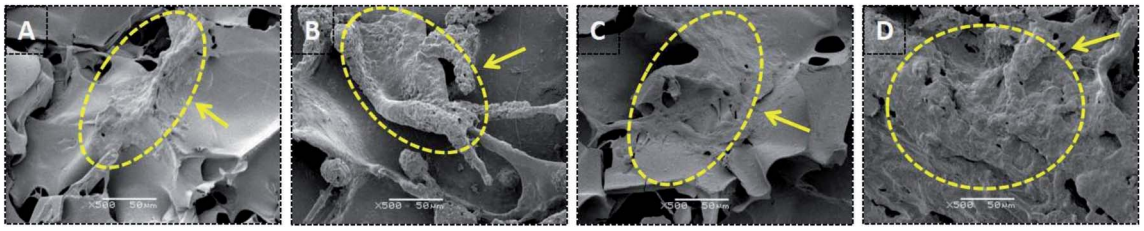

Fig. 5 SEM images of BMSCs cultured on different scaffolds for 10 days. (The dotted areas pointed by the arrow are cell masses surrounded by matrix.) (A) SF (B) SF/nHAp (C) unoriented SF/nHAp/GO (D) Oriented SF/nHAp/GO.

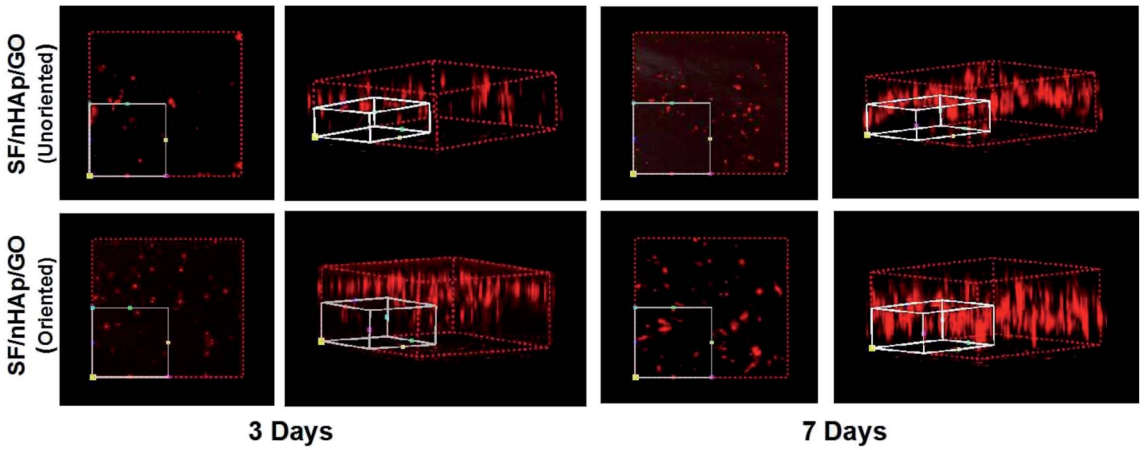

Fig. 7 3-Dimension LSCM images to show HUVECs cultured on the unoriented and oriented SF/nHAp/GO porous scaffolds for 3 and 7 days.

was better than that of the pure SF samples. This certified the ability of nHAp on promoting cell proliferation. But after GO was added, the growth of cells cultured on the unoriented SF/nHAp/GO scaffold slowed down. It seemed to be contrary to our original expectation. As far as we know, a large amount of studies have proved that GO or functionalized GO can support cellular adhesion, proliferation and even induce the differentiation of stem cells. In this study, the effect was not apparent. We speculated that the addition of GO reduced the diameter of pores, then balanced out some effect on promoting cell proliferation with nHAp synergistically. The cell proliferation in oriented SF/nHAp/GO scaffolds confirmed our speculation. It can be seen that there were the same compositions and the same contents between the unoriented and oriented channel-like SF/nHAp/GO porous scaffolds, but the pore size of the latter one was larger than that of the former one, and the porosity of oriented SF/nHAp/GO scaffolds increased due to the existence of channel-like structure. Good scaffolds should facilitate fluid flow, which will allow more uniform distribution of nutrients and facilitate timely delivery of metabolites and scaffold degradation products.

In bone tissue engineering, vascularization of grafts is an important basis for repairing bone defects, and the degree of vascularization is positively correlated with the number of new bone formation.[34,35] Vascular endothelial cells, as main seed cells in studies are a group of multifunctional cells and are also the main cells of angiogenesis. To further confirm that the oriented channel-like structure was conducive to cell proliferation and vascularization, we carried out the second stage of research with HUVECs. 3-D images of cell proliferation in the unoriented and oriented channel-like SF/nHAp/GO porous scaffolds were shown in Fig. 7. Although both scaffolds showed a proliferation trend, it was obviously that scaffolds with orient channel-like structure were more advantageous. At day 7, in the unoriented SF/nHAp/GO scaffolds, the cells basically gathered in the upper and middle pores of the scaffolds, while in the oriented ones, the cells migrated, colonized and proliferated in the unobstructed channels, forming dense vascular cords from the top to the bottom. So, it can be concluded that channel-like structure seemed to mimic the morphology of microvessels, that was beneficial to the proliferation, migration and differentiation of vascular endothelial cells and finally to the formation of new blood vessels. Furthermore, according to CCK8 quantitative test (Fig. 8), with the culture time extension, the proliferation rate of cells on oriented channel-like SF/nHAp/GO porous scaffolds was higher than that of cells on unoriented SF/nHAp/GO ones. This confirmed once again that the channel-like structure could promote cell proliferation and accelerate the process of vascularization, which were conducive to bone regeneration.

3.5 Osteogenic differentiation assay

ALP, one of the phenotypic markers of osteoblasts, is a marker protein to detect the differentiation of stem cells into osteoblasts. Calcium deposition in cell matrix is also a stage specific marker of osteogenesis of stem cells. They are abundantly expressed during the early and late stages of osteogenic

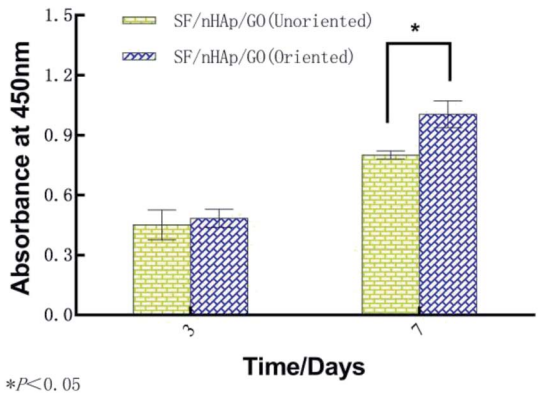

Fig. 8 OD Values of HUVECs cultured on the unoriented and oriented SF/nHAp/GO. Porous scaffolds for 3 and 7 days.

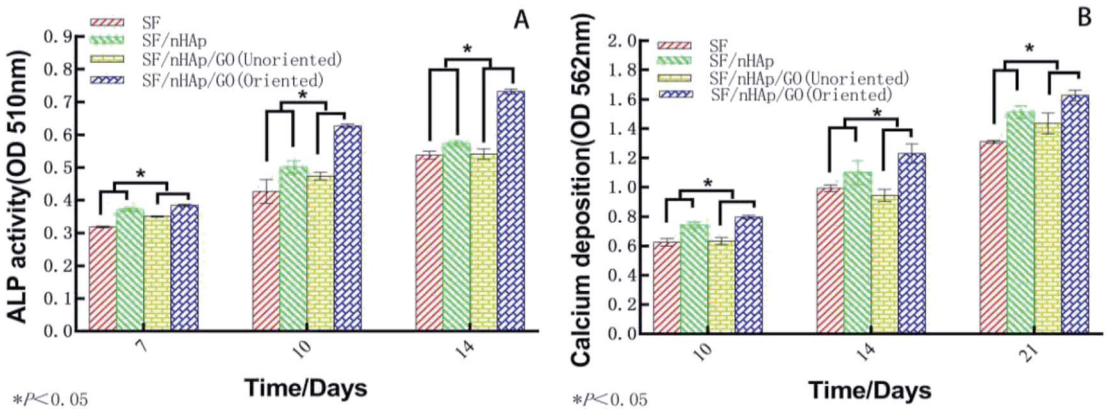

Fig. 9 Alkaline phosphatase in BMSCs cultured on the different scaffolds for 7, 10 and 14 days (A). Calcium deposition in the different scaffolds for 10, 14 and 21 days (B).

differentiation, respectively. So ALP is considered as an early osteoblast activity indicator while calcium deposition as a late one.[36–38] And studies have shown that alizarin red combined with calcium can be redispersed and dissolved in solution by cetylpyridine chloride. Then the absorbance value is measured for semi-quantitative analysis to observe the deposition of calcium in cell matrix so as to judge the degree of osteoblast differentiation more accurately and quantitatively.[39] In this study, ALP activity was assayed on day 7, 10 and day 14 and plotted in Fig. 9A. The results indicated that the ALP activity clearly increased on all the scaffolds from day 7 to 14. In particular, the oriented SF/nHAp/GO group was significantly higher than the other three groups ($P < 0.05$). Similarly, it can be seen that the level of calcium deposition showed an increasing trend from 10 to 21 days and the oriented group expressed a higher level at each stage (Fig. 9B). This result was confirmed by alizarin red staining of whole specimens (Fig. 10). Collectively, the data clearly indicated that the oriented SF/nHAp/GO scaffold not only facilitated cell adhesion, proliferation and vascularization but also accelerated osteogenic differentiation and formation of new bone. Thus, the oriented SF/nHAp/GO scaffold is promising as a potential scaffold to regenerate bone tissue.

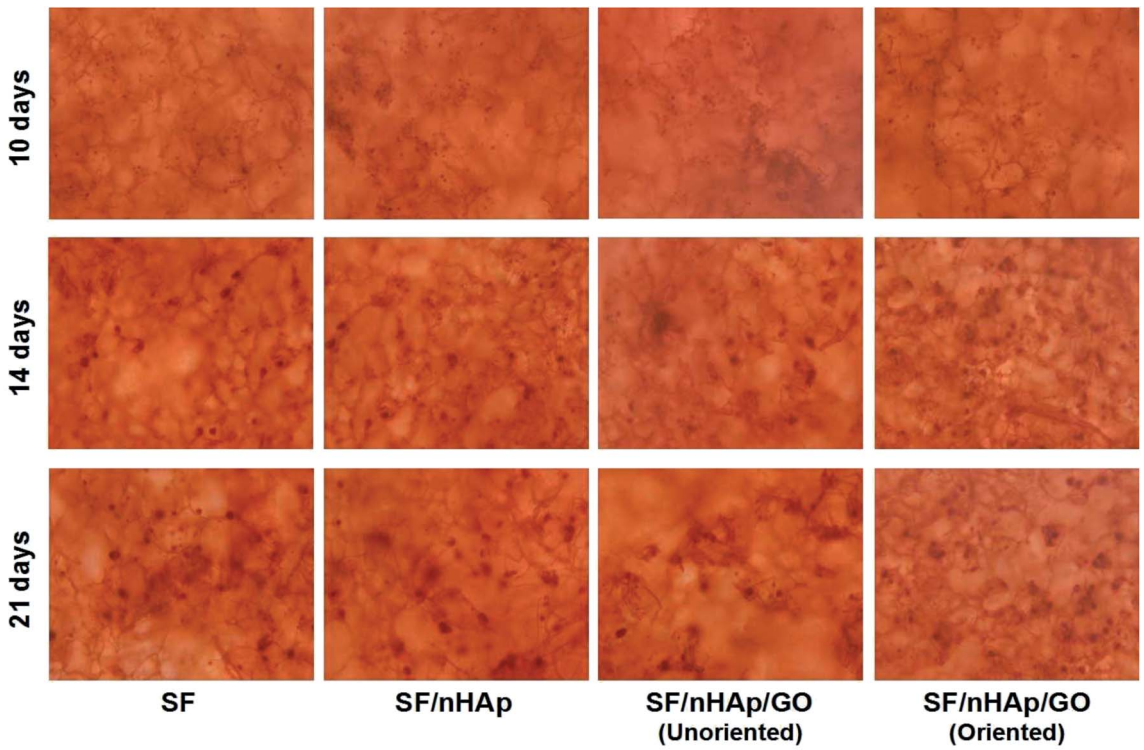

Fig. 10 Alizarin red staining of BMSCs growing on different scaffolds for 14 and 21 days.

4. Conclusion

The combination of SF with fascinating biological effects, nHAp with superior osteogenic activity and GO with robust mechanical property is a competitive approach to make novel scaffolds for orthopedic applications. In this study, a novel oriented channel-like SF/nHAp/GO porous scaffold was successfully fabricated by directional temperature field freezing technology. The nHAp and GO incorporation enhanced the mechanical properties but decreased the pore size to some extent. Cell culture and CCK8 assay indicated that the oriented channel-like SF/nHAp/GO hybrid scaffold had good cell affinity and cytocompatibility. The oriented pore channel with appropriate diameter, high interconnectivity and anisotropic mechanical properties were beneficial for cell to infiltrate into the inner porous structure, which would facilitate vascularization and bone regeneration. Additionally, in the osteoblast differentiation of BMSCs, the oriented channel-like SF/nHAp/GO composite stimulated alkaline phosphatase secretion, and mineral deposition more strongly than the SF, SF/nHAp and traditional spongy SF/nHAp/GO scaffolds. In the future, we will take some further study to illustrate the potential and promise of oriented channel-like SF/nHAp/GO porous scaffold *in vivo*.

Conflicts of interest

The authors declare no conflict of interest.

Acknowledgements

This work was financially supported by Shanxi Key R&D Planning Program (201803D121041), Shanxi Applied Basic Research Program (201701D221065), the Startup Foundation for Doctors of Shanxi Medical University (BS03201638) and follow-up research project of the Fourth National Oral Health Epidemiological Survey (201502002). We gratefully acknowledge the support from Shanxi Province Key Laboratory of Oral Diseases Prevention and New Materials, Clinical Medical Research Center of Oral Diseases of Shanxi Province (Cultivation). We also thank Key Laboratory of Cellular Physiology at Shanxi Medical University, Ministry of Education, and the Department of Physiology, Shanxi Medical University.

Notes and references

1 Q. Lu, X. Hu, X. Q. Wang, J. A. Kluge, S. Z. Lu and D. L. Kaplan, *Acta Biomater.*, 2010, **6**(4), 1380–1387.
2 R. Nazarov, H. J. Jin and D. L. Kaplan, *Biomacromolecules*, 2004, **5**(3), 718–726.
3 U. J. Kim, J. Park, C. M. Li, H. J. Jin, R. Valluzzi and D. L. Kaplan, *Biomacromolecules*, 2004, **5**(3), 786–792.
4 A. Schneider, X. Y. Wang, D. L. Kaplan, J. A. Garlick and C. Egles, *Acta Biomater.*, 2009, **5**(7), 2570–2578.
5 L. Meinel, R. Fajardo, S. Hofmann and D. L. Kaplan, *Bone*, 2005, **37**(5), 688–698.
6 M. Lovett, C. Cannizzaro, L. Daheron, B. Messmer, V. N. Gordana and D. L. Kaplan, *Biomaterials*, 2007, **28**(35), 5271–5279.
7 Q. Zhang, Y. H. Zhao, S. Q. Yan, Y. M. Yang, H. J. Zhao, M. Z. Li, S. Z. Lu and D. L. Kaplan, *Acta Biomater.*, 2012, **8**(7), 2628–2638.
8 S. Q. Yan, Q. Zhang, J. N. Wang, Y. Liu, S. Z. Lu, M. Z. Li and D. L. Kaplan, *Acta Biomater.*, 2013, **9**(6), 6771–6782.
9 T. J. Webster, C. Ergun, R. H. Doremus, R. E. Siegel and R. Bizios, *Biomaterials*, 2001, **22**(11), 1327–1333.
10 K. Fox, P. A. Tran and N. Tran, *Chemphyschem*, 2012, **13**(10), 2495–2506.
11 K. S. Tenhuisen, R. I. Martin, M. Klimkiewicz and P. W. Brown, *J. Biomed. Mater. Res., Part A*, 1995, **29**(7), 803–810.
12 S. S. Kim, M. S. Park, O. Jeon, Y. C. Cha and B. S. Kim, *Biomaterials*, 2006, **27**(8), 1399–1409.
13 R. Y. Zhang and P. X. Ma, *J. Biomed. Mater. Res.*, 2015, **44**(4), 446–455.
14 P. Zheng, Q. Yao, F. Mao, N. Liu, Y. Xu, B. Wei and L. Wang, *Mol. Med. Rep.*, 2017, **16**(4), 5078–5084.
15 X. D. Kong, F. Z. Cui, X. M. Wang, M. Zhang and W. Zhang, *J. Cryst. Growth*, 2004, **270**(1–2), 197–202.
16 H. Y. Liu, J. Cheng, F. J. Chen, D. C. Bai, C. W. Shao, J. Wang, P. X. Xi and Z. Z. Zeng, *Nanoscale*, 2014, **6**(10), 5315–5322.
17 A. D. Dalgic, A. Z. Alshemary, A. Tezcaner, D. Keskin and Z. Evis, *J. Biomater. Appl.*, 2018, 885328218763665.
18 C. Y. Wan and B. Q. Chen, *Biomed. Mater.*, 2011, **6**(5), 055010.
19 M. Li, P. Xiong, F. Yan, S. J. Li, C. H. Ren, Z. C. Yin, A. Li, H. F. Li, X. M. Ji, Y. F. Zheng and Y. Cheng, *Bioact. Mater.*, 2018, **3**(1), 1–18.
20 B. Otsuki, M. Takemoto, S. Fujibayashi, M. Neo, T. Kokubo and T. Nakamura, *Biomaterials*, 2006, **27**(35), 5892–5900.
21 A. C. Jones, C. H. Arns, D. W. Hutmacher, B. K. Milthorpe, A. P. Sheppard and M. A. Knackstedt, *Biomaterials*, 2009, **30**(7), 1440–1451.
22 B. S. Chang, C. K. Lee, K. S. Hong, H. J. Youn, H. C. Ryu, S. S. Chung and K. W. Park, *Biomaterials*, 2000, **21**(12), 1291–1298.
23 G. R. Mitchell and A. Tojeira, *Procedia Eng.*, 2013, **59**, 117–125.
24 L. M. Li, M. H. Zhao, J. D. Li, Y. Zuo, Q. Zou and Y. B. Li, *Mater. Lett.*, 2015, **149**, 25–28.
25 C. Feng, W. J. Zhang, C. J. Deng, G. L. Li, J. Chang, Z. Y. Zhang, X. Q. Jiang and C. T. Wu, *Adv. Sci.*, 2017, **19**, 2847–2850.
26 A. Petersen, A. Princ, G. Korus, A. Ellinghaus, H. Leemhuis, A. Herrera and S. Schreivogel, *Nat. Commun.*, 2018, **9**, 4430.
27 M. Li, P. Xiong, M. S. MO, Y. Cheng and Y. F. Zheng, *Front. Mater. Sci.*, 2016, **10**(3), 1–11.
28 Q. Wang, Y. Y. Chu, J. X. He, W. L. Shao, Y. M. Zhou, K. Qi, L. D. Wang and S. Z. Cui, *Mater. Sci. Eng. C*, 2017, **80**, 232–242.
29 Y. F. Zhang, W. Fan, Z. C. Ma, C. T. Wu, W. Fang, G. Liu and Y. Xiao, *Acta Biomater.*, 2010, **6**(8), 3021–3028.
30 Q. L. Loh and C. Choong, *Tissue Eng. B Rev.*, 2013, **19**(6), 485–502.

31 M. Z. Li, W. Tao, S. Z. Lu and C. X. Zhao, *Polym. Adv. Technol.*, 2008, **19**(3), 207–212.
32 M. Z. Li, M. Ogiso and N. Minoura, *Biomaterials*, 2003, **24**(2), 357–365.
33 J. R. Valverde, *Briefings Bioinf.*, 2001, **2**(2), 199–200.
34 P. Pelissier, F. Villars, S. Mathoulin-Pelissier, R. Bareille and M. H. Lafage-Proust, *Plast. Reconstr. Surg.*, 2003, **111**(6), 1932–1941.
35 T. Tian, T. Zhang, Y. Lin and X. Cai, *J. Dent. Res.*, 2018, 002203451876712.
36 H. Declercq, N. V. Vreken, E. D. Maeyer, R. Verbeeck, E. Schacht, L. D. Ridder and M. Cornelissen, *Biomaterials*, 2004, **25**(5), 757–768.
37 N. I. Zur Nieden, G. Kempka and H. J. Ahr, *Differentiation*, 2003, **71**(1), 18–27.
38 G. M. Stanford, P. A. Jacobson, E. D. Eanes, L. A. Lembke and R. J. Midura, *J. Biol. Chem.*, 1995, **270**(16), 9420–9428.
39 C. Ratisoontorn, M. L. Seto, K. M. Broughton and M. L. Cunningham, *Bone*, 2005, **35**, 627–634.